

The Ω Counter, a Frequency Counter Based on the Linear Regression

Enrico Rubiola, Michel Lenczner, Pierre-Yves Bourgeois, and François Vernotte

Abstract—This paper introduces the Ω counter, a frequency counter—i.e., a frequency-to-digital converter—based on the linear regression (LR) algorithm on time stamps. We discuss the noise of the electronics. We derive the statistical properties of the Ω counter on rigorous mathematical basis, including the weighted measure and the frequency response. We describe an implementation based on a system on chip, under test in our laboratory, and we compare the Ω counter to the traditional Π and Λ counters. The LR exhibits the optimum rejection of white phase noise, superior to that of the Π and Λ counters. White noise is the major practical problem of wideband digital electronics, both in the instrument internal circuits and in the fast processes, which we may want to measure. With a measurement time τ , the variance is proportional to $1/\tau^2$ for the Π counter, and to $1/\tau^3$ for both the Λ and Ω counters. However, the Ω counter has the smallest possible variance, 1.25 dB smaller than that of the Λ counter. The Ω counter finds a natural application in the measurement of the parabolic variance, described in the companion article in this Journal [vol. 63 no. 4 pp. 611–623, April 2016 (Special Issue on the 50th Anniversary of the Allan Variance), DOI 10.1109/TUFFC.2015.2499325].

Index Terms—Frequency estimation, frequency measurement, instrumentation and measurement, noise, phase noise, regression analysis, time measurement.

I. INTRODUCTION AND STATE OF THE ART

THE frequency counter is an instrument that measures the frequency of the input signal versus a reference oscillator. Since frequency and time intervals are the most precisely measured physical quantities, and nowadays, even fairly sophisticated counters fit in a small area of a chip, converting a physical quantity into a frequency is a preferred approach to

Manuscript received June 15, 2015; accepted May 13, 2016. Date of publication May 24, 2016; date of current version July 1, 2016. This work was supported in part by the ANR Programme d'Investissement d'Avenir in progress at the Time and Frequency Departments of CNRS FEMTO-ST Institute and CNRS UTINAM (Oscillator IMP, First-TF, and REFIMEVE+), and in part by the Région de Franche-Comté. ANR is the French Agence Nationale de la Recherche; CNRS is the Centre National de la Recherche Scientifique; FEMTO-ST is the Franche-Comté Electronique Mécanique Thermique et Optique – Sciences et Technologies Institute; UTINAM is the Univers Transport Interfaces Nanostructures Atmosphère et environnement Molécules Laboratory.

E. Rubiola, M. Lenczner, and P.-Y. Bourgeois are with the CNRS FEMTO-ST Institute, Besançon 25030, France (e-mail: rubiola@femto-st.fr; michel.lenczner@femto-st.fr; pyb2@femto-st.fr. Reference author E. Rubiola, home page <http://rubiola.org>).

F. Vernotte is with the CNRS UTINAM Laboratory, Observatory THETA of Franche-Comté, University of Franche-Comté/University of Bourgogne Franche-Comté, 25010 Besançon, France (e-mail: francois.vernotte@obs-besancon.fr).

Digital Object Identifier 10.1109/TUFFC.2016.2570604

the design of electronic instruments. The consequence is that the counter is now such a versatile and ubiquitous instrument that it creates applications rather than being developed for applications, just like the computer.

The term counter comes from the early instruments, where the Dekatron [2]—a dedicated cold-cathode vacuum tube—was used to count the pulses of the input signal in a suitable reference time, say 0.1 or 1 s. While the manufacturers of instruments stick on the word counter, the new terms time-to-digital converter (TDC) and frequency-to-digital converter are often preferred in digital electronics [3], [4].

The direct frequency counter has been replaced long time ago by the classical reciprocal counter, which measures the average period on a suitable interval by counting the pulses of the reference clock. The obvious advantage is that the $1/n$ counts quantization uncertainty is limited by the clock frequency, instead of the arbitrary input frequency. Of course, the clock is set by design close to the maximum toggling frequency of the technology employed.

Higher resolution is obtained by measuring the fractions of the clock period with an interpolator. Simple and precise interpolators work only at fixed frequency. The most widely used techniques are described underneath. Surprisingly, all them are rather old and feature picosecond range resolution. The progress concerns the sampling rate, from kS/s or less in the early time to a few MS/s available now. See [5] for a review, and [3] for integrated electronic techniques.

- 1) The Nutt Interpolator [6], [7] makes use of the linear charge and discharge of a capacitor.
- 2) The Frequency Vernier is the electronic version of the vernier caliper commonly used in the machine shop. A synchronized oscillator close to the clock frequency plays the role of the vernier scale [8]–[11].
- 3) The Thermometer Code Interpolator uses a pipeline of small delay units and D-type flip-flops or latches. To the best of our knowledge, it first appeared in the HP5371A time interval analyzer implemented with discrete delay lines and sparse logic [12].

Table I provides some examples of commercial products.

In the classical reciprocal counter, the input signal is sampled only at the beginning and at the end of the measurement time τ . The frequency measured in this way is averaged over τ with uniform weight. In the presence of time jitter of variance σ_x^2 (classical variance), statistically independent at start and stop, the measured fractional frequency has variance $\sigma_y^2 = 2\sigma_x^2/\tau^2$. Increased resolution can be achieved with fast

TABLE I
SOME COMMERCIAL TDCs AND TIME INTERVAL ANALYZERS

Device / Brand	Resolution	Type	Reference
Acam TDC-GPX	10 ps	Chip	[13]
Carmel Instruments BI201	3 ps	PCI Card	[14]
Guide Tech	1 ps	PCI/PXI Card	[15]
Lange-Electronic GmbH	50 ps	Special purpose	[16], [17]
Keysight 53230A	20 ps	Lab instrument	[18]
Maxim MAX35101	20 ps	Chip	[19]
SPAD Lab TDC	22 ps	Chip	[20]
Stanford Research Systems SR620	25 ps	Lab instrument	[21]
Texas THS788	8 ps	Chip	[22]

sampling and statistics. A sampling interval $\tau_0 = \tau/m$, $m \gg 1$ enables averaging on m highly overlapped and statistically independent measures. In this way, one can expect a variance $\sigma_y^2 \propto \sigma_x^2/m\tau^2$. This mechanism is equivalent to averaging the input frequency with triangular weight. These two methods are referred to as Π and Λ counters (or estimators) because of the graphical analogy of the Greek letter to the weight function [23], [24]. The Π and Λ counters are related to the Allan variance (AVAR) [25], [26] and to the modified Allan variance (MVAR) [27]–[29]. Frequency counters specialized for MVAR are available as a niche product, chiefly for research laboratories [16].

Having access to fast time stamping and to sufficient computing power on field-programmable gate array (FPGA) and system on chip (SoC) at low cost and acceptable complexity, we tackle the problem of the best estimator. The linear regression (LR) turns out to be the right answer, to the extent that it provides the lowest energy (or lowest power) fit of a data set, which is the optimum approximation for white noise.

The LR can be interpreted as a weight function applied to the measured frequency fluctuations. The shape of such weight function is parabolic (Fig. 3). We call the corresponding instrument Ω counter, for the graphical analogy of the parabola with the Greek letter, and in the continuity of the Π and Λ counters [23], [24]. The Ω estimator is similar to the Λ estimator, but exhibits the higher rejection of the instrument noise, chiefly of white phase noise. This is important in the measurement of fast phenomena, where the noise bandwidth is necessarily large.

The idea of the LR for the estimation of frequency is not new [12], [30]. However, these articles lack rigorous statistical analysis. Another modern use of the LR has been proposed independently in [31] at the IEEE international frequency symposium, where we gave our first presentation on the Ω counter and on our standpoint about the parabolic variance (PVAR).

II. INSTRUMENT ARCHITECTURE AND NOISE

The use of time stamps for sophisticated statistics is inspired to the Picket Fence method introduced in [32] and [33], and intended for the JPL time scale. Fig. 1 shows a rather general

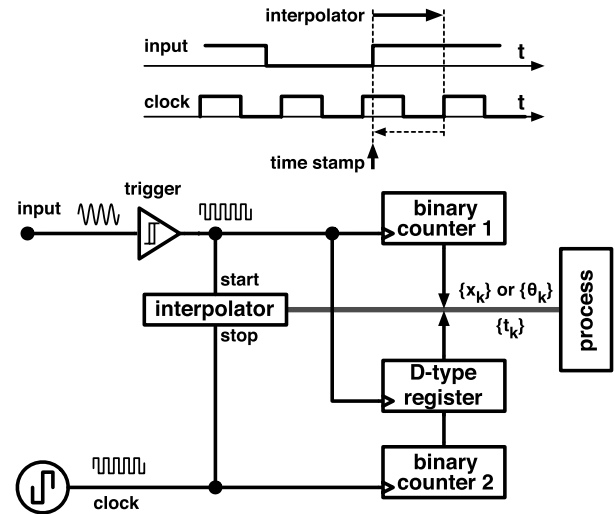


Fig. 1. Time-stamp counter architecture.

block diagram. A time stamp is associated with each input event by combining the integer number of clock cycles (binary counter 2, free running, and sampled by the D-type register) with the fraction of clock cycle, measured by the interpolator. Binary counter 1 counts the input events, and associates the integer number k to the k th event.

Following the signal path, we expect that all the noise originating inside the instrument contains only white and flicker PM noise. The reason is that the instrument internal delay cannot diverge in the long run. Notice that the divergence of the flicker is only an academic issue [34], while the integral of $S_\varphi(f) = \mathbf{b}_{-1}/f$ over an interval of 20–40 decades of frequency (unrealistically large) exceeds the coefficient \mathbf{b}_{-1} by a mere 16–20 dB. Conversely the reference oscillator—which in a strict sense is not a part of the instrument—and the signal under test include white FM and slower phenomena. The analysis of practical cases, underneath, shows that the instrument internal noise is chiefly white PM.

A. Internal Clock Distribution

The reference clock signal is distributed to the critical parts of the counters by appropriate circuits. As an example, we evaluate the jitter of the Cyclone III FPGA by Altera [35]. A reason is that we have studied thoroughly the noise of this device [36]. Another reason is that it is the representative of the class of midsized FPGAs, and similar devices from other brands, chiefly Xilinx [37], would give similar results.

White phase noise is of the aliased φ -type, described by

$$S_\varphi(f) = \frac{a^2}{\nu_0}$$

where ν_0 is the clock frequency, and $a \approx 630 \mu\text{rad}$ is an experimental parameter of the component. Since the PM noise is sampled at the threshold crossings, i.e., at $2\nu_0$, the bandwidth is equal to ν_0 . Converting $S_\varphi(f)$ into $S_x(f) = (1/4\pi^2\nu_0^2)S_\varphi(f)$ and integrating on ν_0 , we get

$$\langle x^2 \rangle = \frac{a^2}{4\pi^2\nu_0^2}$$

thus $x_{\text{rms}} = 1$ ps at 100-MHz clock frequency.

Flicker phase noise is of the x -type. We measured 22 fs/ $\sqrt{\text{Hz}}$ at 1 Hz, referred to 1-Hz bandwidth. Integrating over 12–15 decades, we find 115–130-fs rms, which is low as compared with white noise.

B. Input Trigger

In most practical cases, the noise is low enough to avoid multiple bounces at the threshold crossings [38]. In this condition, the rms time jitter is

$$x_{\text{rms}} = \frac{V_{\text{rms}}}{\text{SR}}$$

where V_{rms} is the rms fluctuation of the threshold, and SR is the slew rate (slope, not accounting for noise).

The rms voltage results from white and flicker noise. White noise is described as $V_w = e_n \sqrt{B}$, where e_n is the white noise in 1-Hz bandwidth and B is the noise bandwidth. Flicker noise results from $V_f = \alpha e_n (\ln(B/A))^{1/2}$, where αe_n is the flicker noise at 1 Hz and referred to 1-Hz bandwidth, and A and B are the low and high cutoff frequencies, respectively.

The golden rules for precision high-speed design suggest the following.

- 1) White noise, $e_n = 10$ nV/ $\sqrt{\text{Hz}}$, including the input protection circuits (without, it would be of 1–2 nV/ $\sqrt{\text{Hz}}$).
- 2) Flicker noise, $\alpha = 10 \dots 31.6$ (20–30 dB) at most, as a conservative estimate.
- 3) The noise bandwidth is related to the maximum input (toggling) frequency ν_{max} by $\nu_{\text{max}} \simeq 0.3$ B.

Let us consider a realistic example where $\nu_{\text{max}} = 1.2$ GHz, $e_n = 10$ nV/ $\sqrt{\text{Hz}}$, and $\alpha = 31.6$ (30 dB). Accordingly, the input bandwidth is $B = 4$ GHz. In turn, the integrated white noise is $V_w = 632$ μV rms. By contrast, flicker is $V_f = 1.66$ μV rms integrated over 12 decades (4 MHz to 4 GHz), and $V_f = 1.86$ μV rms integrated over 15 decades (4 μHz to 4 GHz). White noise is clearly the dominant effect.

C. Clock Interpolator

Commercially available counters exhibit the single-shot fluctuation of 1–50 ps (Table I, and references therein). Since the interpolator is reset to its initial state after each use, it is sound to assume that the noise realizations are statistically independent. This is white noise. At a closer sight, some memory between operations is possible, which shows up as flicker noise. However, the issues about bandwidth already discussed in this section apply, and we expect that the flicker is a minor effect as compared with white noise.

D. Motivation for the Linear Regression

The LR finds a straightforward application to the estimation of the frequency ν of a periodic phenomenon $\sin[\phi(t)]$ from its phase $\phi(t)$ using the trite relation $\nu = (1/2\pi)(d\phi/dt)$. It is well known that the LR provides the best estimate $\hat{\nu}$ in the presence of white noise, to the extent that it minimizes the squared residuals. The reader can refer to [39, Gauss–Markov theorem] or to the classical book [40]. Notice that the samples

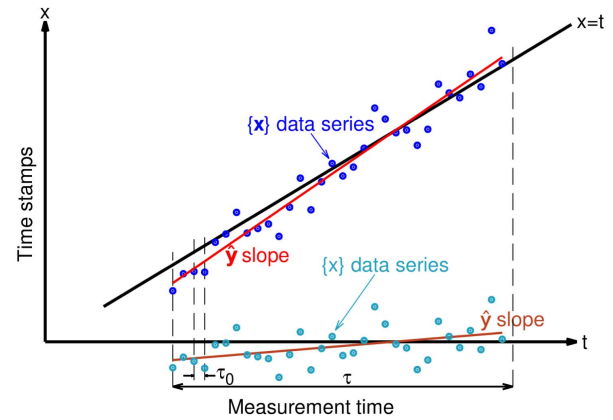


Fig. 2. Principle of the LR counter, and definition of often used variables.

of white noise are statistically independent, because in this case, the noise autocorrelation is a Dirac δ distribution. This property matches the need of rejecting the white phase noise.

III. LINEAR REGRESSION

A real sinusoidal signal affected by noise can be written as

$$v(t) = V_0 \sin[\phi(t)]$$

where V_0 is the amplitude and $\phi(t)$ is a phase that carries the ideal time plus random noise. The randomness in $\phi(t)$ can be interpreted either as a phase fluctuation or as a frequency fluctuation

$$\phi(t) = \begin{cases} 2\pi \nu_0 t + \varphi(t) & \text{(PM noise)} \\ 2\pi \nu_0 t + 2\pi \int (\Delta\nu)(t) dt & \text{(FM noise)} \end{cases}$$

and, of course, $\phi(t)$ and $\varphi(t)$ are allowed to exceed $\pm\pi$. Hereinafter, ν_0 is either the nominal frequency or its best estimate. The difference is relevant only to the absolute accuracy, while we can analyze the fluctuation assuming that the average is equal to zero.

We prefer to derive the properties of the LR using the normalized quantities $\mathbf{x}(t)$ and $\mathbf{y}(t)$, as in Fig. 2

$$\mathbf{x}(t) = t + x(t) \quad \text{(phase time)} \quad (1)$$

$$\mathbf{y}(t) = 1 + y(t) \quad \text{(fractional frequency)} \quad (2)$$

where

$$\mathbf{x}(t) = \varphi(t)/2\pi \nu_0 \quad (3)$$

$$\mathbf{y}(t) = \dot{\mathbf{x}}(t). \quad (4)$$

The quantity $\mathbf{x}(t)$ is the time carried by the real signal, which is equal to the ideal time t plus the random fluctuation $x(t)$. The quantities $\mathbf{x}(t)$ and $\mathbf{y}(t)$ match the phase time fluctuation $x(t)$ and the fractional frequency fluctuation $y(t)$ used in the general literature [25], [26], with the choice of the font as the one and only difference. The random variables \mathbf{x} and \mathbf{y} are centered, so the mathematical expectation of \mathbf{x} and \mathbf{y} is t and 1, respectively.

Most concepts are suitable to continuous and discrete treatise with simplified notation. For example, $\mathbf{x} = t + x$ maps

into $\mathbf{x}_k = t_k + \mathbf{x}_k$ for sampled data, and into $\mathbf{x}(t) = t + \mathbf{x}(t)$ in the continuous case. The notation $\langle \cdot \rangle$ and (\cdot, \cdot) stands for the average and the scalar product. They are defined as $\langle x \rangle = (1/n) \sum_k x_k$ and $(x, y) = \sum_k x_k y_k$ for time series, where n is the number of terms in the sum, and defined as $\langle x \rangle = (1/T) \int x(t) dt$ and $(x, y) = (1/T) \int x(t)y(t) dt$ in the continuous case, where T is the integration time. The span of the sum and the integral will be made precise in each application. The reader may notice that the factor $1/T$ in the continuous (x, y) does not find the $1/n$ counterpart in the discrete (x, y) . This difference in the normalization is necessary for consistency with the companion article [1]. The norm is defined as $\|\mathbf{x}\| = (\mathbf{x}, \mathbf{x})^{1/2}$. The mathematical expectation and the variance of random variables are denoted by $\mathbb{E}\{\cdot\}$ and $\mathbb{V}\{\cdot\}$.

The problem of the LR consists in identifying the optimum value $\hat{\mathbf{y}}$ of the slope η (dummy variable used to avoid confusion with \mathbf{y}) that minimizes the norm of the error $\mathbf{x} - \eta t$. The solution is the random variable

$$\hat{\mathbf{y}} = \frac{(\mathbf{x} - \langle \mathbf{x} \rangle, t - \langle t \rangle)}{\|t - \langle t \rangle\|^2}. \quad (5)$$

The choice of a reference system where the time sequence is centered at zero, i.e., $\langle t \rangle = 0$, makes the treatise simpler, without loss of generality. Accordingly, the estimator $\hat{\mathbf{y}}$ reads

$$\hat{\mathbf{y}} = \frac{(\mathbf{x}, t)}{\|t\|^2}. \quad (6)$$

These choices are equivalent, because $\langle t \rangle = 0$, so $(\mathbf{x} - \langle \mathbf{x} \rangle, t) = (\mathbf{x}, t) - \langle \mathbf{x} \rangle (1, t) = (\mathbf{x}, t)$.

IV. BASIC STATISTICAL PROPERTIES

A. Unbiased Estimate

The LR provides an unbiased estimate of the slope, that is

$$\mathbb{E}\{\hat{\mathbf{y}}\} = 1 \quad (\text{unbiased estimate})$$

even without the assumption that the noise samples (or values) are statistically independent. This is seen by replacing the expression of the phase

$$\hat{\mathbf{y}} = \frac{(\mathbf{x}, t)}{\|t\|^2} = \frac{(t + \mathbf{x}, t)}{\|t\|^2} = 1 + \frac{(\mathbf{x}, t)}{\|t\|^2}.$$

Since t is deterministic, $\mathbb{E}\{(\mathbf{x}, t)\} = (\mathbb{E}\{\mathbf{x}\}, t)$ implies

$$\mathbb{E}\{\hat{\mathbf{y}}\} = 1 + \frac{(\mathbb{E}\{\mathbf{x}\}, t)}{\|t\|^2} = 1$$

because we assumed $\mathbb{E}\{\mathbf{x}\} = 0$.

B. Estimator Variance

We restrict the analysis of the estimator variance to the discrete case. In fact, the continuous case is more about an academic exercise that a practical issue because continuous is the extrapolation of discrete for infinite sampling frequency ($\tau_0 \rightarrow 0$). The variance of white noise diverges, which is compensated by $m \rightarrow \infty$. Alternatively, we have to introduce a finite noise bandwidth, thus correlation in the white noise.

Introducing the hypothesis that the samples \mathbf{x}_k are independent, the estimator variance is

$$\mathbb{V}\{\hat{\mathbf{y}}\} = \frac{\sigma_{\mathbf{x}}^2}{\|t\|^2} \quad (\text{estimator variance}).$$

This is seen by expanding the variance

$$\mathbb{V}\{\hat{\mathbf{y}}\} = \mathbb{E}\{(\hat{\mathbf{y}} - \mathbb{E}\{\hat{\mathbf{y}}\})^2\} = \mathbb{E}\{\hat{\mathbf{y}}^2\} - \mathbb{E}\{\hat{\mathbf{y}}\}^2.$$

But

$$\begin{aligned} \mathbb{E}\{(\hat{\mathbf{y}})^2\} &= \frac{1}{\|t\|^4} \mathbb{E}\{(t + \mathbf{x}, t)^2\} \\ &= \frac{1}{\|t\|^4} \mathbb{E}\{(t, t)^2 + 2(t, t)(\mathbf{x}, t) + (\mathbf{x}, t)^2\} \\ &= 1 + \frac{1}{\|t\|^4} \mathbb{E}\{(\mathbf{x}, t)^2\}. \end{aligned}$$

In the case of uniformly spaced time series, and exploiting the fact that the random variables \mathbf{x}_k are independent, we find

$$\mathbb{E}\{(\mathbf{x}, t)^2\} = \sum_{k, \ell} t_k t_\ell \mathbb{E}\{\mathbf{x}_k \mathbf{x}_\ell\} = \sum_k t_k^2 \mathbb{E}\{\mathbf{x}_k^2\} = \|t\|^2 \sigma_{\mathbf{x}}^2.$$

We conclude that

$$\mathbb{V}\{\hat{\mathbf{y}}\} = 1 + \frac{\|t\|^2}{\|t\|^4} \sigma_{\mathbf{x}}^2 - 1 = \frac{\sigma_{\mathbf{x}}^2}{\|t\|^2}.$$

For a constant step τ_0 and with $\tau = m\tau_0$, then for large m , it holds that

$$\begin{aligned} \hat{\mathbf{y}} &\approx 1 + \frac{12(\mathbf{x}, t)}{m\tau^2} \\ \mathbb{V}\{\hat{\mathbf{y}}\} &\approx \frac{12\sigma_{\mathbf{x}}^2}{m\tau^2}. \end{aligned} \quad (7)$$

For even $m = 2p$, the proof starts with $t_k = k\tau_0$ for $k \in \{-p, \dots, p\}$

$$\begin{aligned} \|t\|^2 &= \sum_{k=-p}^p t_k^2 = \tau_0^2 \sum_{k=-p}^p k^2 = 2\tau_0^2 \sum_{k=1}^p k^2 \\ &= \frac{\tau_0^2}{3} p(2p+1)(p+1) = \frac{\tau_0^2}{12} m(m+2)(m+1) \\ &\approx \frac{m\tau^2}{12} \quad \text{for large } m. \end{aligned}$$

A similar calculation with odd $m = 2p+1$ takes $t_k = (k + (1/2)\tau_0)$ for $k \in \{-p-1, \dots, p\}$, and gives the same result.

V. WEIGHTED AVERAGE AND FILTERING

We show that the Ω counter can be described as a weighted average or as a filter, and we derive the impulse response from the weight function. Only the continuous case is analyzed, because the discrete case can be treated in the same way. Unlike Section IV-B, the extension is smooth and free from singularities.

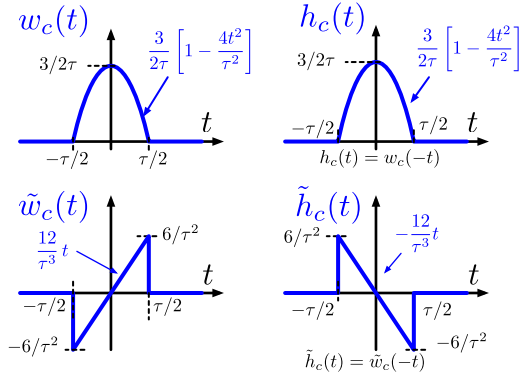


Fig. 3. Weight functions and impulse response of the Ω counter.

A. Weighted Measure

Let us consider an instrument that measures $\mathbf{y}(t)$ averaged on a time interval of duration τ . In general terms, we can express the estimate $\hat{\mathbf{y}}(t)$ available at the time t as the weighted average

$$\hat{\mathbf{y}}(t) = \int_{\mathbb{R}} \mathbf{y}(s) w_c \left(s - t + \frac{\tau}{2} \right) ds \quad (8)$$

where the weight function $w_c(t)$ is ruled by

$$w_c(t) = 0 \text{ for } t \notin \left(-\frac{\tau}{2}, \frac{\tau}{2} \right) \quad (\text{support})$$

$$\int_{\mathbb{R}} w_c(t) dt = 1 \quad (\text{normalization}).$$

This states that the integral (8) has duration τ ending at the time t , and that the normalization yields a valid average. The subscript c stands for centered. Accordingly, $w_c(\cdot)$ is shifted by $\tau/2$ in (8).

Interestingly, (8) can be seen as a scalar product, as a linear operator on \mathbf{y} , as a measure in the sense of the mathematical measure theory, and, of course, as a weighted measure as physicists and engineers are familiar with.

We identify the function $w_c(t)$ starting with a function $\tilde{w}_c(t)$, which satisfies

$$\hat{\mathbf{y}}(t) = \int_{\mathbb{R}} \mathbf{x}(s) \tilde{w}_c \left(s - t + \frac{\tau}{2} \right) ds. \quad (9)$$

Then, recalling that $\mathbf{y}(t) = \dot{\mathbf{x}}(t)$ and using the integration-by-part formula $\int f(t)g'(t) dt = -\int f'(t)g(t) dt$, we find

$$w_c(t) = -\int_{-\infty}^t \tilde{w}_c(s) ds. \quad (10)$$

Equation (9) gives the estimate at the time $\tau/2$

$$\hat{\mathbf{y}}(\tau/2) = \int_{-\tau/2}^{\tau/2} \mathbf{x}(t) \tilde{w}_c(t) dt. \quad (11)$$

The LR (6) applied over $(-\tau/2, \tau/2)$ and the computation of $\|t\|^2 = \tau^3/12$ give

$$\hat{\mathbf{y}}(\tau/2) = \frac{(\mathbf{x}, t)}{\|t\|^2} = \frac{12}{\tau^3} \int_{-\tau/2}^{\tau/2} \mathbf{x}(t) t dt. \quad (12)$$

Comparing (11) and (12), we find

$$\tilde{w}_c(t) = \begin{cases} \frac{12}{\tau^3} t, & \text{for } t \in \left(-\frac{\tau}{2}, \frac{\tau}{2} \right) \\ 0, & \text{elsewhere} \end{cases} \quad (13)$$

and using (10)

$$w_c(t) = \begin{cases} \frac{3}{2\tau} \left[1 - \frac{4t^2}{\tau^2} \right], & \text{for } t \in \left(-\frac{\tau}{2}, \frac{\tau}{2} \right) \\ 0, & \text{elsewhere.} \end{cases}$$

These functions are plotted in Fig. 3 (left).

B. Frequency Response

For the general experimentalist, the noise rejection properties of the counter are best seen in the frequency domain. The fluctuations $\mathbf{y}(t)$ and $\mathbf{x}(t)$ are described in terms of their single-sided power spectral densities (PSDs) $S_{\mathbf{y}}(f)$ and $S_{\mathbf{x}}(f)$, and the counter as a linear time-invariant (LTI) system, which responds with its output fluctuation $\hat{\mathbf{y}}(t)$. The counter output PSD is

$$S_{\hat{\mathbf{y}}}(f) = |H_c(f)|^2 S_{\mathbf{y}}(f)$$

$$S_{\hat{\mathbf{y}}}(f) = |\tilde{H}_c(f)|^2 S_{\mathbf{x}}(f)$$

where $|H_c(f)|^2$ and $|\tilde{H}_c(f)|^2$ are the frequency response for frequency noise and for phase noise, respectively.

The LTI system theory teaches us that $H_c(f)$ is the Fourier transform of the impulse response $h_c(t)$

$$H_c(f) = \int_{\mathbb{R}} h_c(t) e^{-i2\pi f t} dt$$

and so $\tilde{h}_c(t) \leftrightarrow \tilde{H}_c(f)$. The subscript c in $h_c(t)$ and $\tilde{h}_c(t)$ stands for centered (left shifted by $\tau/2$), and propagates to the frequency domain for notation consistency. However, a time shift has no effect on $|H_c(f)|^2$ and $|\tilde{H}_c(f)|^2$.

We start from the time-domain response of the estimator, which results from the convolution integral

$$\hat{\mathbf{y}}(t) = \mathbf{y}(t) * h_c(t) = \int_{\mathbb{R}} \mathbf{y}(s) h_c(t-s) ds.$$

A direct comparison of the above to (8) gives $h_c(t) = w_c(-t)$, hence [Fig. 3 (right)]

$$h_c(t) = \begin{cases} \frac{3}{2\tau} \left[1 - \frac{4t^2}{\tau^2} \right], & \text{for } t \in \left(-\frac{\tau}{2}, \frac{\tau}{2} \right) \\ 0, & \text{elsewhere} \end{cases}$$

and

$$H_c(f) = -\frac{3}{\pi^3 f^3 \tau^3} [\pi f \tau \cos(\pi f \tau) - \sin(\pi f \tau)]$$

$$|H_c(f)|^2 = \frac{9}{\pi^6 f^6 \tau^6} [\pi f \tau \cos(\pi f \tau) - \sin(\pi f \tau)]^2.$$

In the same way, comparing the convolution integral

$$\hat{\mathbf{y}}(t) = \mathbf{x}(t) * \tilde{h}_c(t) = \int_{\mathbb{R}} \mathbf{x}(s) \tilde{h}_c(t-s) ds$$

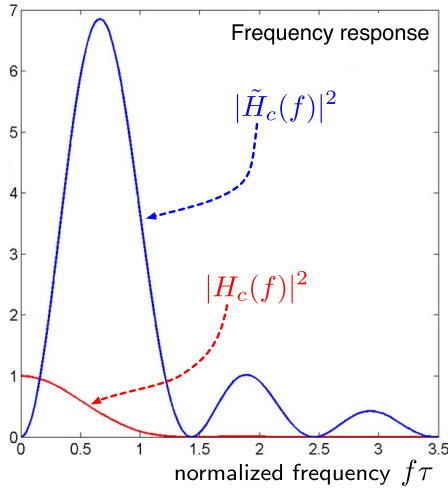


Fig. 4. Frequency response of the Ω counter.

to (9) yields $\tilde{h}_c(t) = \tilde{w}_c(-t)$. There follows [Fig. 3 (right)]:

$$\tilde{h}_c(t) = \begin{cases} -\frac{12}{\tau^3}t, & \text{for } t \in (-\frac{\tau}{2}, \frac{\tau}{2}) \\ 0, & \text{elsewhere} \end{cases} \quad (14)$$

and

$$\tilde{H}_c(f) = -\frac{6i}{\pi^2 f^2 \tau^3} [\pi f \tau \cos(\pi f \tau) - \sin(\pi f \tau)]$$

$$|\tilde{H}_c(f)|^2 = \frac{36}{\pi^4 f^4 \tau^6} [\pi f \tau \cos(\pi f \tau) - \sin(\pi f \tau)]^2.$$

The transfer functions $|H_c(f)|^2$ and $|\tilde{H}_c(f)|^2$ are shown in Fig. 4.

VI. HARDWARE TECHNIQUES

We describe a hardware implementation based on a Xilinx Zedboard. This is a demo board for the Zynq chip, an SoC consisting of an FPGA, and a CPU. At the present time, only the LR algorithm is implemented. It features a sampling rate of up to 250 MS/s, i.e., $\tau_0 \geq 4$ ns, independent on the block size m .

Fig. 5 shows the block diagram. The algorithm takes two steps, represented as stages, running simultaneously on contiguous blocks of m data (a power of two). The reason for the two stages is that the evaluation of $\hat{\nu}$ needs all the samples of the block and the average. The first stage calculates the average and transfers the data stream to the RAM, while the second stage calculates the LR coefficients. So, the output is available at a rate $1/\tau$. An additional delay of τ applies at startup, because data have to propagate through the two stages.

Dropping the normalization, the LR calculates the frequency

$$\hat{\nu} = \frac{\sum_{k=0}^{m-1} (\theta_k - \langle \theta_k \rangle) (t_k - \langle t_k \rangle)}{\sum_{k=0}^{m-1} (t_k - \langle t_k \rangle)^2} \quad (15)$$

by fitting the phase data $\theta_k = \phi_k/2\pi$, expressed as the fraction of period. It is worth mentioning that, for a given m , the series $\{t_k\}$ and its average $\langle t_k \rangle$ can be calculated and stored in RAM.

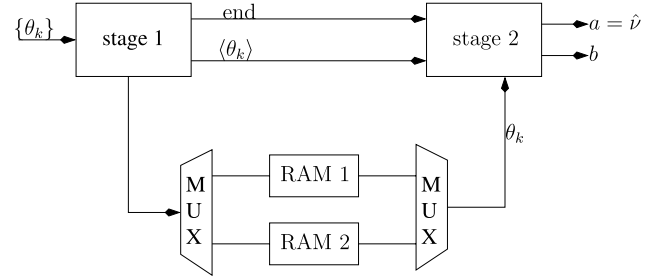


Fig. 5. Hardware implementation.

A. First Stage

1) *Data Transfer*: A block of data θ_k , sampled at the rate $\nu_s = 1/\tau_0$, is transferred to the external dual-port RAM.

2) *Accumulation*: Each of the m values θ_k is encoded on M bits, stored on the left half of a $2M$ -b register, right-shifted by the gain $g = \log_2(m)$, and added to a $2M$ -b accumulator. At the end, the value stored in the accumulator is equal to the average. Provided that $g \leq M$, there is no roundoff error.

3) *Next Cycle*: Data transfer and accumulation are simultaneous, which takes a time equal to $\tau = m\tau_0$. When the first RAM is full and the average is available, an end-of-process signal is sent, and the results are propagated to the second stage. A new cycle starts, with the next m samples stored in the second RAM.

B. Second Stage

1) *Difference Calculation*: The samples are collected from the RAM, and $\theta_i - \langle \theta_k \rangle$ is calculated. In parallel, the values of $t_i - \langle t_k \rangle$ are also computed, with $\langle t_k \rangle$ provided by the CPU. The calculation of $t_i - \langle t_k \rangle$ takes no additional RAM. All data are latched.

2) *Frequency Estimation*: This process is the asynchronous accumulation of $\sum_{k=0}^{m-1} (\theta_k - \langle \theta_k \rangle) (t_k - \langle t_k \rangle)$. The slope a is obtained by dividing this sum by the denominator of (15). Finally, $\hat{\nu}$ is latched, resized, and sent to the output. For practical reasons, we also estimate the intercept $b = \langle \theta_k \rangle - a \langle t_k \rangle$.

C. Oracle

First, we checked on mechanical errors by comparing the results with those obtained from independent C-language code. The latter is a fixed-point implementation equivalent to the GNU-Octave LR function, or to the Levenberg–Marquardt algorithm, found, for example, in Gnuplot.

Second, we evaluate the chip resources. The main cause of area occupation is the RAM, which is linearly proportional to m . With large m , we also need larger word size M in order to prevent roundoff errors. Large RAM usage may lead to long propagation time, thus to potential data corruption. The number of 48-b arithmetic units is not an issue, because it grows slowly with m . Table II summarizes the FPGA resources needed in some cases. An LR over 32 kSamples is a good deal in the most practical cases, considering that the sampling frequency ν_s can be slowed down. If this is not sufficient, one has to consider larger FPGAs.

TABLE II
Zynq RESOURCE USAGE

word size M	block size m	RAM		DSP units	
		blocks	%	no	%
32	1024	2/140	1.4	4/220	1.8
32	2^{15}	64/140	45	4/220	1.8
64	2^{15}	128/140	91.4	13/220	5.9

VII. DISCUSSION

A. Noise Rejection

We summarize the noise response of the counters in the presence of a data series $\{\mathbf{x}_k\}$ uniformly spaced by τ_0 , or equivalently sampled at the frequency $\nu_s = 1/\tau_0$. The measurement time is $\tau = m\tau_0$, and the noise samples \mathbf{x}_k associated with \mathbf{x}_k are statistically independent.

The analysis of the Π and Λ counters provided in this section is based on [23] and [24], with a notation difference concerning the Λ counter. In [23] and [24], the measurement time spans over 2τ and two contiguous measures are overlapped by τ . This choice is driven by the application to the MVAR, having the same response $\text{mod}\sigma_y^2(\tau) = (1/2)\mathbf{D}_y^2\tau^2$ to a constant drift \mathbf{D}_y . Oppositely, in this paper, we use the same time interval $\tau = m\tau_0$ for all the counters, and we leave the two-sample variances to the companion article [1].

1) *Π Counter*: The estimated fractional frequency is

$$\hat{\mathbf{y}} = \frac{\mathbf{x}_{m-1} - \mathbf{x}_0}{m\tau_0} = \frac{\mathbf{x}_{m-1} - \mathbf{x}_0}{\tau}.$$

The associated variance is

$$\mathbb{V}\{\hat{\mathbf{y}}\} = \frac{2\sigma_{\mathbf{x}}^2}{m^2\tau_0^2} = \frac{2\sigma_{\mathbf{x}}^2}{\tau^2} \quad (16)$$

independent of the sampling frequency.

2) *Λ Counter*: In the measurement time $\tau = m\tau_0$, we average $m/2$ almost-overlapped samples \mathbf{y}_k each of which is measured by Π counter over a time $\tau/2$

$$\hat{\mathbf{y}}_k = \frac{\mathbf{x}_{m/2+k} - \mathbf{x}_k}{m\tau_0/2} = \frac{\mathbf{x}_{m/2+k} - \mathbf{x}_k}{\tau/2}.$$

The variance associated with each \mathbf{y}_k is

$$\mathbb{V}\{\hat{\mathbf{y}}_k\} = \frac{2\sigma_{\mathbf{x}}^2}{m^2\tau_0^2/4}.$$

The Λ estimator gives $\hat{\mathbf{y}} = (2/m) \sum_{k=0}^{(m-1)/2} \mathbf{y}_k$. Thus, the estimator variance is

$$\mathbb{V}\{\hat{\mathbf{y}}\} \approx \frac{16\sigma_{\mathbf{x}}^2}{m^3\tau_0^2} = \frac{16\sigma_{\mathbf{x}}^2}{\nu_s\tau^3}. \quad (17)$$

3) *Ω Counter*: The estimator variance (7) can be written as

$$\mathbb{V}\{\hat{\mathbf{y}}\} \approx \frac{12\sigma_{\mathbf{x}}^2}{m^3\tau_0^2} = \frac{12\sigma_{\mathbf{x}}^2}{\nu_s\tau^3}. \quad (18)$$

4) *Comparison*: Comparing the estimator variance $\mathbb{V}\{\hat{\mathbf{y}}\}$ as given by (16)–(18), we notice that the Π estimator features the poorest rejection to white PM noise, proportional to $1/\tau^2$. The white PM noise rejection follows the $1/\tau^3$ law for both the Λ and Ω estimators, but the Ω estimator is more favorable by a factor of 3/4, i.e., 1.25 dB. However small, this benefit comes at no expense in terms of the complexity of precision electronics.

The sampling frequency $\nu_s = 1/\tau_0$ can be equal to the input frequency ν_0 or an integer fraction of, depending on the speed of the interpolator and on the data transfer rate. Values of 1–4 MHz are found in commercial equipment.

B. Data Decimation

We address the question of decimating a stream $\{\mathbf{y}_k\}$ of contiguous data averaged over τ , in order to get a new stream $\{\mathbf{y}_j\}$ of contiguous data averaged over $n\tau$, and preserving the statistical properties of the estimator.

1) *Π Counter*: Decimation is trivially done by averaging n contiguous data with zero dead time

$$\hat{\mathbf{y}}(n\tau) = \frac{1}{n} \sum_{k=0}^{n-1} \hat{\mathbf{y}}_k(\tau).$$

2) *Λ Counter*: Decimation can be done in powers of 2, provided that contiguous samples are overlapped by exactly $\tau/2$. In this case, we apply recursively the formula

$$\hat{\mathbf{y}}(2\tau) = \frac{1}{4}\hat{\mathbf{y}}_{-1}(\tau) + \frac{1}{2}\hat{\mathbf{y}}_0(\tau) + \frac{1}{4}\hat{\mathbf{y}}_1(\tau).$$

Notice that the overlap between samples yields a measurement time equal to 2τ .

3) *Ω Counter*: An exact decimation formula was not found yet. The reason is that the parabolic shape has the constant second derivative, and edges at $\pm\tau/2$. Indeed, the problem is under study.

C. Application to the Two-Sample Variances

The general form of the two-sample variance reads

$$\mathbb{V}\{\hat{\mathbf{y}}\} = \frac{1}{2}\mathbb{E}\{(\hat{\mathbf{y}}_1 - \hat{\mathbf{y}}_2)^2\}. \quad (19)$$

Using a stream of contiguous data $\{\hat{\mathbf{y}}_k\}$ measured with a Π , a Λ , or a Ω estimator, (19) gives the AVAR, the MVAR, or the PVAR. In the case of the MVAR, contiguous means 50% overlapped.

VIII. CONCLUSION

The architecture shown in Fig. 1 is suitable to the Π , Λ , and Ω estimators, just by replacing the algorithm. So, smart design enables to implement the three estimators in a single instrument.

The Π estimator is the poorest, and mentioned only for completeness. Nonetheless, it is still on the stage when extreme simplicity is required, or in niche applications, such as the measurement of the AVAR for long-term timekeeping.

The Λ estimator is a good choice when a clean decimation of the output data is mandatory.

In the presence of white noise, the Ω estimator is similar to the Λ estimator, but features smaller variance by a factor of 3/4 (1.25 dB). However the reader may not regard a factor of 3/4 a major improvement, the value of the Ω counter is in the optimum estimator in the presence of white noise, that is, the minimum square residuals (residual energy). We recall that the white noise has a dominant role in wide bandwidth systems.

If complexity is the major issue, the Λ estimator fits. Oppositely, if the ultimate noise performance in the presence of wideband noise is an issue, the Ω estimator is the right answer. In addition, the Ω estimator outperforms the Λ estimator in the detection of all noise phenomena from white PM to random walk FM [1]. The complexity of the LR is likely to be affordable on FPGA or SoC electronics.

ACKNOWLEDGMENT

The authors would like to thank the members of the Go Digital Working Group at FEMTO-ST and UTINAM for stimulating discussions, and G. Goavec-Merou for support with FPGA programming.

REFERENCES

- [1] F. Vernotte, M. Lenczner, P.-Y. Bourgeois, and E. Rubiola, "The parabolic variance (PVAR): A wavelet variance based on the least-square fit," *IEEE Trans. Ultrason., Ferroelectr., Freq. Control*, vol. 63, no. 4, pp. 611–623, Apr. 2016.
- [2] Ericsson Telephones Ltd. Dayton, OH, USA.(1955). *GC10B, GC10B/S (CV2271) Scale-of-Ten Counters*, accessed on Jun. 2016. [Online]. Available: <http://www.decadecounter.com/vta/pdf1/GC10B.pdf>
- [3] S. Henzler, *Time-to-Digital Converters*. New York, NY, USA: Springer, 2010.
- [4] S. Yoder, M. Ismail, and W. Khalil, *VCO-Based Quantizers Using Frequency-to-Digital and Time-to-Digital Converters*. New York, NY, USA: Springer, 2011.
- [5] J. Kalisz, "Review of methods for time interval measurements with picosecond resolution," *Metrologia*, vol. 41, no. 1, pp. 17–32, 2004.
- [6] R. Nutt, "Digital time intervalometer," *Rev. Sci. Instrum.*, vol. 39, no. 9, pp. 1342–1345, Sep. 1968.
- [7] R. Nutt, K. Milam, and C. W. Williams, "Digital intervalometer;" U.S. Patent 3 983 481, Sep. 28, 1976.
- [8] C. Cottini and E. Gatti, "Millimicrosecond time analyzer," *Nuovo Cimento*, vol. 4, no. 6, pp. 1550–1557, Dec. 1956.
- [9] C. Cottini, E. Gatti, and G. Giannelli, "Millimicrosecond time measurements based upon frequency conversion," *Nuovo Cimento*, vol. 4, no. 1, pp. 156–157, Jul. 1956.
- [10] H. W. Lefevre, *The Vernier Chronotron*. Chicago, IL, USA: Univ. Michigan Library, Jan. 1957.
- [11] P. J. Kindlmann and J. Sunderland, "Phase stabilized vernier chronotron," *Rev. Sci. Instrum.*, vol. 37, no. 4, pp. 445–452, Apr. 1966.
- [12] D. C. Chu, "Phase digitizing: A new method for capturing and analyzing spread-spectrum signals," *Hewlett Packard J.*, vol. 40, no. 2, pp. 28–35, Feb. 1989.
- [13] TDCs – Time-to-Digital Converters, Germany. *ACAM Messelectronic GmbH, 76297 Stutensee-Blankenloch*, accessed on Jun. 2016. [Online]. Available: <http://www.acam.de/products/time-to-digital-converters/>
- [14] Carmel Instruments LLC, Campbell, CA, USA. *BI201 Time Interval Analyzer / Counter*, accessed on Jun. 2016. [Online]. Available: <http://www.carmelinst.com/Default.aspx>
- [15] GuideTech, Santa Clara, CA, USA. *Computer-Based Instruments*, accessed on Jun. 2016. [Online]. Available: <http://www.guidetech.com/computer-based-instruments.html>
- [16] G. Kramer and K. Klische, "Multi-channel synchronous digital phase recorder," in *Proc. IEEE Int. Freq. Control Symp.*, Seattle WA, USA, Jun. 2001, pp. 144–151.
- [17] Lange-Electronic GmbH. Germlinden, Germany, accessed on Jun. 2016. [Online]. Available: <http://lange-electronic.de/index.php/en/>
- [18] Keysight Technologies, Inc., Santa Rosa, CA, USA. (Jan. 2015). *53200A Series RF/Universal Frequency Counter/ Timers*, accessed on Jun. 2016. [Online]. Available: <http://keysight.com>
- [19] Maxim Integrated, San Jose, CA, USA. (Jan. 2015). *MAX35101 Time-to-Digital Converter With Analog Front-End*, accessed on Jun. 2016. [Online]. Available: <http://www.maximintegrated.com>
- [20] SPAD Lab, Politecnico di Milano, Italy. *TDC (Time to Digital Converter)*, accessed on Jun. 2016. [Online]. Available: <http://www.everyphotoncounts.com/ic-tdc.php>
- [21] Stanford Research Systems, Sunnyvale, CA, USA. (Feb. 2006). *SR620 Universal Time Interval Counter*, accessed on Jun. 2016. [Online]. Available: <http://www.thinksrs.com>
- [22] Texas Instruments Inc., Dallas, TX, USA. (Mar. 2015). *THS788 Quad Channel Time Measurement Unit*, accessed on Jun. 2016. [Online]. Available: <http://www.ti.com>
- [23] E. Rubiola, "On the measurement of frequency and of its sample variance with high-resolution counters," *Rev. Sci. Instrum.*, vol. 76, no. 5, May 2005, Art. no. 054703.
- [24] S. T. Dawkins, J. J. McFerran, and A. N. Luiten, "Considerations on the measurement of the stability of oscillators with frequency counters," *IEEE Trans. Ultrason., Ferroelectr., Freq. Control*, vol. 54, no. 5, pp. 918–925, May 2007.
- [25] D. W. Allan, "Statistics of atomic frequency standards," *Proc. IEEE*, vol. 54, no. 2, pp. 221–230, Feb. 1966.
- [26] J. A. Barnes *et al.*, "Characterization of frequency stability," *IEEE Trans. Instrum. Meas.*, vol. IM-20, no. 2, pp. 105–120, May 1971.
- [27] J. J. Snyder, "Algorithm for fast digital analysis of interference fringes," *Appl. Opt.*, vol. 19, no. 8, pp. 1223–1225, Apr. 1980.
- [28] D. W. Allan and J. A. Barnes, "A modified 'Allan variance' with increased oscillator characterization ability," in *Proc. 35 IFCS*, Fort Monmouth, NJ, USA, May 1981, pp. 470–474.
- [29] P. Lesage and T. Ayi, "Characterization of frequency stability: Analysis of the modified Allan variance and properties of its estimate," *IEEE Trans. Instrum. Meas.*, vol. 33, no. 4, pp. 332–336, Dec. 1984.
- [30] S. Johansson, "New frequency counting principle improves resolution," in *Proc. IEEE Int. Freq. Control Symp. Expo.*, Vancouver, BC, Canada, Aug. 2005, pp. 628–635.
- [31] E. Benkler, C. Lisdat, and U. Sterr. (Apr. 2015). "On the relation between uncertainties of weighted frequency averages and the various types of Allan deviations." [Online]. Available: <http://arxiv.org/pdf/1504.00466v3.pdf>
- [32] C. A. Greenhall, "A method for using a time interval counter to measure frequency stability," *IEEE Trans. Ultrason., Ferroelectr., Freq. Control*, vol. 36, no. 5, pp. 478–480, Sep. 1989.
- [33] C. A. Greenhall, "The third-difference approach to modified Allan variance," *IEEE Trans. Instrum. Meas.*, vol. 46, no. 3, pp. 696–703, Jun. 1997.
- [34] F. Vernotte and E. Lantz, "Metrology and 1/f noise: Linear regressions and confidence intervals in flicker noise context," *Metrologia*, vol. 52, no. 2, pp. 222–237, 2015. [Online]. Available: <http://stacks.iop.org/0026-1394/52/i=2/a=222>
- [35] Altera Corp., San Jose, CA, USA. *Cyclone III FPGAs*, accessed on Jun. 2016. [Online]. Available: <http://altera.com>
- [36] C. E. Calosso and E. Rubiola, "Phase noise and jitter in digital electronic components (invited article)," in *Proc. Int. Freq. Control Symp.*, Taipei, Taiwan, May 2014, pp. 532–534.
- [37] Xilinx, Inc., San Jose, CA, USA. *FPGAs & 3D ICs*, accessed on Jun. 2016. [Online]. Available: <http://www.xilinx.com>
- [38] E. Rubiola, A. Del Casale, and A. De Marchi, "Noise induced time interval measurement biases," in *Proc. Int. Freq. Control Symp.*, Hershey, PA, USA, May 1992, pp. 265–269.
- [39] B. S. Everitt, *The Cambridge Dictionary of Statistics*, 2nd ed. Cambridge, U.K.: Cambridge Univ. Press, 2002.
- [40] H. Cramér, *Mathematical Methods of Statistics*. Princeton, NJ, USA: Princeton Univ. Press, 1946.



Enrico Rubiola received the M.S. degree in electronics engineering from the Politecnico di Torino, Turin, Italy, in 1983, the Ph.D. degree in metrology from the Italian Ministry of Scientific Research, Rome, Italy, in 1989, and the D.Sc. degree in time and frequency metrology from the University of Franche-Comté (UFC), Besançon, France, in 1999.

He has been a Researcher with the Politecnico di Torino, a Professor with the University of Parma, Parma, Italy, and Université Henri Poincaré, Nancy, France, and a Guest Scientist with the NASA Jet Propulsion Laboratory, Pasadena, CA, USA. He has been a Professor with UFC and a Scientist with the Centre National de la Recherche Scientifique, Franche Comté Électronique Mécanique Thermique et Optique-Sciences et Technologies Institute, Besançon, since 2005, where he currently serves as the Deputy Director of the Time and Frequency Department. He has also investigated various topics of electronics and metrology, namely, navigation systems, time and frequency comparisons, atomic frequency standards, and gravity. He is the PI of the Oscillator IMP project, a platform for the measurement of short-term frequency stability and spectral purity. His current research interests include precision electronics, phase-noise, amplitude-noise, frequency stability and synthesis, and low-noise oscillators from the low RF region to optics.



Michel Lenczner received the M.S. and Ph.D. degrees in numerical analysis from the University of Paris VI, Paris, France, in 1987 and 1991, respectively.

He was an Associate Professor of Applied Mathematics with the University of Franche-Comté, Besançon, France. He is currently a Professor of Mechanical Engineering with the Technical University of Belfort-Monbéliard, Belfort, France, and a Researcher with the Micro-Acoustics Team, Franche Comté Électronique Mécanique Thermique et Optique-Sciences et Technologies Institute, Besançon. His current research interests include multiscale modeling and control of distributed mechatronic systems with an emphasis on micro and nanosystems.



Pierre-Yves Bourgeois was born in Besançon, France, in 1976. He received the Ph.D. degree from the University of Franche-Comté (UFC), Besançon, in 2004.

He studied ultrastable microwave cryogenic sapphire resonator oscillators with the Laboratoire de Physique et de Métrologie des Oscillateurs, UFC. After the postdoctoral appointment with the Frequency Standards and Metrology Research Group, University of Western Australia, Crawley WA, Australia, he joined the Time and Frequency Department, Centre National de la Recherche Scientifique, Franche-Comté Électronique Mécanique Thermique et Optique-Sciences et Technologies Institute, Besançon. He is currently involved in investigating the definition of digital methods applied to the modern techniques of time and frequency metrology and to the development of high precision instruments. His current research interests include atomic oscillators and trapped-ion clocks.

Dr. Bourgeois received the IEEE Ultrasonics, Ferroelectrics, and Frequency Control Society Best Student Award in 2004 for the development of ultralow drift cryogenic sapphire oscillators.



François Vernotte received the Ph.D. degree in engineering sciences from the University of Franche-Comté (UFC), Besançon, France, in 1991.

He has been with the Time and Frequency Team, Observatory THETA/UTINAM, UFC, since 1989. His favorite tools are statistical data processing (time series and spectral analysis), parameter estimation (inverse problem and Bayesian statistics), and simulation (Monte-Carlo). His current research interests include long-term stability of oscillators, such as atomic clocks and millisecond pulsars.